Citation: Barba, S., M. M. C. Carafa, and E. Boschi (2008), Experimental evidence for mantle drag in the Mediterranean, *Geophys. Res. Lett.*, 35, L06302, doi:10.1029/2008GL033281.

Experimental evidence for mantle drag in the Mediterranean

Salvatore Barba [1], Michele M. C. Carafa, [1,2] and Enzo Boschi [1,3]

[1]Istituto Nazionale di Geofisica e Vulcanologia, Rome, Italy.

[2]Dipartimento di Scienze della Terra, Universita` "G. D'Annunzio," Chieti, Italy.

[3]Settore Geofisica, Dipartimento di Fisica, Universita` di Bologna, Bologna, Italy.

Abstract

What forces control active deformation in the Central Mediterranean? Slab-pull has long been debated, but no other hypothesis has been generally accepted. Here we analyze the role of shear basal tractions.

By using a thin-shell modeling technique, we generated a large number of models that span different sets of boundary conditions from the literature; we then explored acceptable ranges of model parameters. We computed residuals between model predictions and several datasets of stress directions, GPS measurements and tectonic stress regimes that have been produced in recent studies, and then compared the best models obtained in the presence of tractions with those obtained in the absence of tractions.

For all tested boundary conditions and all considered datasets, our results show that the only successful models are those with significant basal shear traction exerted by eastward mantle flow.

Citation: Barba, S., M. M. C. Carafa, and E. Boschi (2008), Experimental evidence for mantle drag in the Mediterranean, *Geophys. Res. Lett.*, 35, L06302, doi:10.1029/2008GL033281.

Introduction

Mantle flow acts as a tectonic force and is generally considered to resist plate motion [Forsyth and Uyeda, 1975]. However, dynamic models show, at least in North America, the Caribbean and Tonga [Liu and Bird, 2002; Negredo et al., 2004; Conder and Wiens, 2007], that the mantle drags the overlying plates. Also, global models suggest that mantle flows eastward [Doglioni, 1990; Smith and Lewis, 1999] and controls the hinge migration of west-dipping subductions [Doglioni et al., 2007]. In the context of the Central Mediterranean, Africa-Europe convergence explains only part of the observations, such as the crustal shortening across Sicily and the Alps. In contrast, the opening of the Tyrrhenian basin [Royden, 1988], the polarization of fast S-waves [Margheriti et al., 2003] and the existence of low-angle normal faults [Barchi et al., 1998] require an additional force that is distinct from slab pull [Negredo et al., 1999; Barba, 1999; Carminati et al., 2001]. In this study, we quantitatively and systematically compared the active and resistive mantle-flow scenarios in the Central Mediterranean. To this end, we developed a finite element model and analyzed, under a number of boundary conditions, the misfits between model predictions and a large amount of surface data. Our procedure iterates over a selection of boundary conditions and parameters that reproduce those published in the scientific literature. Those model results that exhibited the lowest misfits with the data were averaged, thereby accounting for uncertainties in boundary conditions and model parameters and permitting us to evaluate the reliability of the results.

We found that basal shear tractions, possibly exerted by mantle flow, are required both in the Northern Apennines and in the Calabrian Arc.

Method and Data

We modeled the Central Mediterranean Area (Figure 1) using the finite-element code SHELLS developed by Bird [1999, and references therein]. SHELLS incorporates faults and realistic rheology in a two-layer grid (crust and lithospheric mantle) with laterally-varying thickness, heat flow and topography. It solves the horizontal components of the momentum equation to predict long-term horizontal velocities, anelastic strain rates, vertically integrated stresses, and fault slip rates.

Our grid consists of 5126 triangular continuum elements and 822 fault elements. The vertical integrals are performed using 1-km-steps at each of seven Gauss integration points in each finite element (continuum or fault). For faults, we adopted 109 individual faults and 67 composite seismogenic sources (Figure 2) from DISS v.3.0.2 [DISS Working Group, 2006] which are based on geological and geophysical data and which are capable of M≥5.5 earthquakes [Basili et al., 2008]. We represented composite sources as a single fault trace assuming the dip from the database and the strike from the surface projection of the composite source. Thus, we surmounted the assumptions related to the identification of individual earthquake sources (e.g., segmentation, characteristic behavior). We also incorporated active faults not included in DISS database. We set the effective fault friction to 0.3 although we tested the range 0.15-0.6. For crust and lithosphere thicknesses, values from the literature were adopted [Aichroth, 1990; Nicolich, 2001; Marone et al., 2003; Calcagnile and Panza, 1981; Babuska and Plomerova, 2006].

The steady-state heat flow or the Moho temperature were derived from the literature [Pasquale et al., 1997; Pasquale et al., 1999; Verdoya et al., 2005]. Where we had no information, we interpolated, assuming a heat flow of 0.060 W/m^2 at the model edges. The final heat flow represents a filtered flux that only marginally depends on non-stationary components (e.g., meteoric water circulation, erosion and sedimentation).

Some quantities were set to be uniform in the crust/mantle by assuming regional averages. We set the densities (at 275 K) to 2850/3350 Kg/m^3, the volumetric thermal expansion coefficients to $0/3.5 \times 10^{-5}$ K^{-1}, the thermal conductivities to 3/3.4 $Wm^{-1}K^{-1}$ and the constant radioactive heat production to $8 \times 10^{-7}/0$ K^{-1}. For dislocation creep, we computed the shear stress from $\sigma_s^{creep} = A\dot{e}_s \exp\left(\frac{B+Cz}{T}\right)$, where $\dot{e}_s$ is the shear strain rate, T is the temperature, z is the depth, $A=2.11 \times 10^6/1.28 \times 10^4$ Pa $s^{1/3}$, B=8625/18028 K and C=0/0.017. We set the plasticity limit, i.e., the shear stress above which the strain does not increase, to 500 MPa.

We applied a number of boundary conditions derived from the literature to the five segments of the model perimeter, and tested all their possible combinations in the Eurasia reference frame for a total of 64

cases. The following is a list of the tested boundary conditions: Europe (EU; fixed), Adria (AD; 1: fixed, 2: orthogonally fixed, 3 and 4: NE convergence with respect to Eurasia [Serpelloni et al., 2005; Westaway, 1990); Africa (AF; 1: NE EU-convergence [Serpelloni et al., 2007], 2: NW EU-convergence [Mantovani et al., 2007]); Ionio (IO; 1: AF-fixed, 2: AD-fixed, 3: subject to lithostatic stress only, and 4: EU convergence [Westaway, 1990]); EU-AF transition zone (TR; 1: AF-fixed and 2: reflection symmetry across the North-AF thrust). To simulate the effect of the eastward mantle flow, we applied arc-normal shear tractions from 0-100 MPa at the base of the model beneath the Apennines and the Calabrian Arc (Figure 2). These tractions are located where the maximum force is transferred to the lithosphere, i.e., where mantle encounters continental lithosphere.

Comparisons with observations

To evaluate the quality of the modeling results, we compared the model predictions with four independent datasets: geodetic horizontal velocities from temporary and permanent GPS stations, the stress regime data, based on relative stress magnitudes, and the directions of maximum horizontal compressive stress.

Model-predicted horizontal velocities were compared with 129 geodetic data: 56 from both permanent and temporary stations [Serpelloni et al., 2007] and 73 from permanent stations only (28 from the EUREF and 45 from the Italian-Austrian permanent GPS networks; Caporali, 2007). For simplicity, the two datasets will be referred to as “temporary” and “permanent”, respectively. All geodetic data use the ITRF2000 datum definition.

To constrain the stress regimes and the stress directions in the Andersonian conditions, we used data taken from Montone et al. [2004]. Such data are derived from borehole break-outs, M≥4 earthquake fault-plane solutions, composite focal mechanisms and faults. We use ~200 SH_{max} orientations of good quality (labeled A and B), and ~400 stress regime data.

In general, the “best” model is the one that simultaneously minimizes the L1 or L2 misfit norm between model predictions and all available datasets. However, no model totally satisfies this condition, because minimizing a misfit relative to one dataset can result in increasing the misfit with another dataset.

In all cases, the choice of the "best" model therefore remains a somewhat arbitrary decision. To reduce arbitrariness, we combined all misfits together into a synthetic index (I_s) by weighing each misfit relative to the others based on known uncertainties. Misfits were then standardized using the formula:

$$I_s = \sum_i \frac{(e_i - e_i^{min})}{e_i^{dev}}$$

where e_i are the different misfits, e_i^{min} are the reached minimum misfits and e_i^{dev} are the standard deviations of the misfits that are less than a certain cut-off value. This procedure leads us to define discretional cut-off values, below which we consider the misfits to be acceptable. To deal with Gaussian GPS residuals and spiky stress outliers, we used the L2 norm for GPS data and the L1 norm for stress data. Cutoff values of σ^{temp}=3 mm/a, σ^{perm}=2 mm/a, $\Delta\theta$=33° and $\%_{bad}$=20% were adopted, and the resulting I_s for our models was

$$I_S = \frac{\left(\sigma_{u,v}^{temp} - 1.64\,\text{mm/a}\right)}{\left(0.134\,\text{mm/a}\right)} + \frac{\left(\sigma_{u,v}^{perm} - 1.09\,\text{mm/a}\right)}{\left(0.133\,\text{mm/a}\right)} + \frac{\left(\Delta\vartheta - 23°\right)}{\left(2.3°\right)} + \frac{\left(\%_{bad} - 9.63\%\right)}{\left(2.7\%\right)}$$

In order to compare the models with tractions to the models without tractions, we analyzed how the tractions affected the I_s with varying boundary conditions and validation datasets (Figure 3).

Results and Discussion

To verify the hypothesis of the existence of basal tractions in the Central Mediterranean, we produced a large number of models that spanned different sets of boundary conditions and explored the acceptable ranges of model parameters. We computed residuals between model predictions and several datasets, and then compared the best models obtained in the presence of tractions with those obtained in the absence of tractions.

We found that all sets of boundary conditions followed the same pattern, which was characterized by a clear reduction in misfits between measured and predicted values when applying eastward basal tractions, regardless of the chosen dataset (Figure 3). Dealing with the 50-models average allowed us to compute the error on model predictions and helped our procedure to find a global minimum. The null hypothesis is rejected at 3% significance level. In contrast, all the applied boundary conditions failed to reproduce important tectonic features in the absence of tractions.

Although the Africa-Eurasia convergence reproduced well the stress directions and GPS velocities in Sicily and in the Southern Tyrrhenian, it inhibited extension in the Apennines with SE-trending SH_{max}. Models with counterclockwise rotation of Adria, as proposed by Westaway [1990] or Serpelloni et al. [2005], showed the correct orientation of stress axes, but did not reproduce the extension-compression pair in the Apennines. Conversely, models with basal tractions were able both to generate the extension-compression pair in the Apennines and to predict larger NW velocity vectors in Apulia than those in the Northern Apennines. The basal tractions also predicted the correct orientations of SH_{max}, thereby reproducing the stress field along the Apennines and the peri-Tyrrhenian region (Figure 4). For all the analyzed boundary conditions, basal tractions clearly reduced residuals (Figure 3a).

We found that the best models without tractions had misfits of σ^{temp}=1.85 mm/a, σ^{perm}=1.31 mm/a, $\Delta\theta$=28.85°, $\%_{bad}$=16.35% and I_s =2.31, whereas models with tractions had lower misfits of σ^{temp}=1.64 mm/a, σ^{perm}=1.10 mm/a, $\Delta\theta$=24.27°, $\%_{bad}$=10.04% and I_s =0.95.

Only models with active mantle flow proved to be successful, indicating that inner lithospheric forces do not suffice to reproduce the observed data. However, more work is necessary to improve the determination of the magnitude, direction, spatial distribution and geodynamic significance of the basal tractions. Although we assumed uniform basal traction, stress and GPS data are not uniformly distributed. Consequently, we could not verify the model predictions in areas where data was more scarce, such as the Central-Southern Adriatic shoreline. Also, our models did not reproduce the Po plain data well; this is because we applied uniform basal tractions where the Apennines actually bends at its Northern termination.

Although we cannot clearly differentiate broad scale mantle flow from wedge induced flow, we favor the mantle flow for the northern Apennines, as in Doglioni et al. [2007], and the mantle wedge for the Calabrian Arc, as in Faccenna et al. [2005]. In the Northern Apennines, the tractions rotated the direction of SH_{max} and generated compression at the outer thrust, whereas in the Calabrian Arc, the tractions generated arc-normal extension, despite the arc-parallel velocities. However, the upper-asthenosphere viscosity greatly affected the geodynamic processes. In the viscosity range 10^{20}-10^{12} Pa s, basal tractions are ascribed to mantle drag (high viscosity), trench suction (intermediate) and slab pull

(low viscosity) [Doglioni et al., 2007]. The existence of an eastward mantle flow relative to the lithosphere is also in agreement with the interpretation of the surface-wave tomography by Panza et al. [2007]. They showed that the low-velocity layer in the upper asthenosphere is well stratified and confined beneath the old northern Africa continental lithosphere, whereas it is rather dispersed in the Apennines back-arc. All these observations agree well with a shallow upper mantle convection/circulation in the Tyrrhenian and a contemporaneous eastward flow, regardless of whether this flow is a cause or an effect of the slab retreat. Furthermore, the E-W trending of the anisotropy directions in the Tyrrhenian region and their abrupt rotation [Margheriti et al., 2003] suggest that a flow can exist and interact with the lithosphere. Differences in the magnitude of the seismic anisotropy between northern and southern Italy [Baccheschi et al., 2007] suggest that uniform flow is an oversimplified assumption.

In our deformable model, the basal tractions generated the apparent rotation of Adria, and rigid plate behavior was not required. This fact argues for new criteria to be adopted in the interpretation of GPS data in the Mediterranean. The arc-normal predicted orientation of stress axes favors the hypothesis that the external thrusts are active, which justifies the occurrence of reverse faulting earthquakes along the Adriatic margin [Basili and Barba, 2007] and also implies that the seismic potential of the Ionian thrust should be better studied.

We conclude that basal horizontal forces are required to reproduce surface observations in the Central Mediterranean. Misfits between model predictions and surface data were significantly reduced when tractions were used, regardless of the datasets and boundary conditions applied.

Acknowledgments. We are grateful to Peter Bird for making available the source code of SHELLS and to Roberto Basili and Gianluca Valensise for support and discussions. The article benefited of the careful reading by H. Bungum and J.A. Conder. MMCC fellowship was funded by the Italian Civil Defense through INGV-DPC Project S2.

References

Aichroth, B. (1990), The European geotraverse seismic refraction experiment of 1986 from Genoa, Italy, to Kiel, Germany, *Tectonophysics*, *176*(1-2), 43-57.

Babuska, V., and J. Plomerova (2006), European mantle lithosphere assembled from rigid microplates with inherited seismic anisotropy, *Physics of Earth and Planetary Interiors*, 158, 264–280.

Baccheschi, P., L. Margheriti, and M. S. Steckler (2007), Seismic anisotropy reveals focused mantle flow around the Calabrian slab (Southern Italy), *Geophys. Res. Lett.*, *34*, L05302, doi:10.1029/2006GL028899.

Barba, S. (1999), Studio dei meccanismi di deformazione della regione italiana: vincoli geologici, geofisici e modellazione geodinamica (in Italian), Ph.D. thesis, 100 pp., University of Roma. (Available at http://hdl.handle.net/2122/367)

Barchi, M., G. Minelli, and G. Pialli (1998), The Crop 03 profile: a synthesis of results on deep structures of the Northern Apennines, in *Results of the CROP03 deep seismic reflection profile*, edited by G. Pialli, M. Barchi and G. Minelli, *Mem. Soc. Geol. It.*, 52, 383-400.

Basili, R., and S. Barba (2007), Migration and shortening rates in the northern Apennines, Italy: implications for seismic hazard, *Terra Nova*, doi: 10.1111/j.1365-3121.2007.00772.x.

Basili, R, G. Valensise, P. Vannoli, P. Burrato, U. Fracassi, S. Mariano, M. M. Tiberti, and E. Boschi (2008), The Database of Individual Seismogenic Sources (DISS), version 3: summarizing 20 years of research on Italy's earthquake geology, *Tectonophysics,* doi: doi:10.1016/j.tecto.2007.04.014.

Bird, P. (1999), Thin-plate and thin-shell finite-element programs for forward dynamic modeling of plate deformation and faulting, *Computers & Geosciences*, *25*(4), 383-394.

Calcagnile, G. and G. F. Panza (1981), The main characteristics of the lithosphere-asthenosphere system in Italy and surrounding, *Pure and Applied Geophysics*, Vol. 119, N. 4, 865-879.

Caporali, A. (2007), Geophysical characterization of the main seismogenic structures, in *Final reports of the project "Assessing the Seismogenic Potential and the Probability of Strong Earthquakes in Italy"*, edited by D. Slejko and G. Valensise, pp. 25-42, Ist. Naz. di Geofis. e Vulcanol., Rome. (Available at http://hdl.handle.net/2122/3090)

Carminati, E., F. Toniolo Augier and S. Barba (2001), Dynamic modelling of stress accumulation in Central Italy: role of structural heterogeneities and rheology, *Geophysical Journal International*, *144*(2), 373-390.

Conder, J. A., and D. A. Wiens (2007), Rapid mantle flow beneath the Tonga volcanic arc, *EPSL, 264, 299-307.*

DISS Working Group (2006), Database of Individual Seismogenic Sources (DISS), Version 3.0.2: A compilation of potential sources for earthquakes larger than M 5.5 in Italy and surrounding areas, http://www.ingv.it/DISS/. (Available at http://hdl.handle.net/2122/2412)

Doglioni, C. (1990), The global tectonic pattern, *Journal of Geodynamics, 12(1)*, 21-38.

Doglioni, C., E. Carminati, M. Cuffaro, and D. Scrocca (2007), Subduction kinematics and dynamic constraints, *Earth Science Reviews, 83(3-4)*, 125-175.

Faccenna C., L. Civetta, M. D'Antonio, F. Funiciello, L. Margheriti, and C. Piromallo (2005), Constraints on mantle circulation around the deforming Calabrian slab, *Geophys. Res. Lett., 32 (6)*, L06311.

Forsyth, D. and S. Uyeda (1975), On the relative importance of the driving forces of plate motions, Geophys. J. R. Astron. Soc., 43, 163-200.

Liu, Z., and P. Bird (2002), North America plate is driven westward by lower mantle flow, *Geophys. Res. Lett., 29*(24), 2164.

Mantovani, E., M. Viti, D. Babbucci, and D. Albarello (2007), Nubia-Eurasia kinematics: an alternative interpretation from Mediterranean and North Atlantic evidence, *Ann. Geophys.,* 50(3), 341-366.

Margheriti, L., F. P. Lucente, and S. Pondrelli (2003), SKS splitting measurements in the Apenninic-Tyrrhenian domain (Italy) and their relation with lithospheric subduction and mantle convection, *Journal of Geophysical Research-Solid Earth*, *108*(B4), 20.

Marone, F., M. van der Meijde, and S. van der Lee (2003), Joint inversion of local, regional and teleseismic data for crustal thickness in the Eurasia-Africa plate boundary region, *Geophysical Journal International*, *154*(2), 499-514

Montone, P., M. T. Mariucci, S. Pondrelli, and A. Amato (2004), An improved stress map for Italy and surroundings regions (Central Mediterranean), *Journal of Geophysical Research, Vol. 109*(B), 10410.

Negredo, A.M., E. Carminati, S. Barba, R. and Sabadini (1999), Dynamic modelling of stress accumulation in central Italy *Geophysical Research Letters, 26,* 1945-1948.

Negredo, A.M., I. Jimenez-Munt, and A. Villasenor (2004), Evidence for eastward mantle flow beneath the Caribbean plate from neotectonic modeling, *Geophysical Research Letters*, *31*(6), 4.

Nicolich, R. (2001), Deep Seismic Transects, in *Anatomy of an orogen: the Appennines and Adjacent Mediterranean Basins*, edited by G. B. Vai and P. Martini, Kluver Acad. Publischers, 47-52.

Panza, G.F., R.B. Raykova, E. Carminati, and C. Doglioni (2007), Upper mantle flow in the western Mediterranean. *Earth Planet. Sci. Lett., 257,* 200-214.

Pasquale, V., M. Verdoya, P. Chiozzi, and G. Ranalli (1997), Rheology and seismotectonic regime in the northern central Mediterranean , *Tectonophysics, Vol. 270*, 239-257.

Pasquale, V., M. Verdoya, and P. Chiozzi (1999), Thermal state and deep earthquakes in the Southern Tyrrhenian, *Tectonophysics, Vol. 306*, 435–448.

Royden, L. (1988), Flexural behavior of the continental lithosphere in Italy: Constraints imposed by gravity and deflection data, *J. Geophys. Res., 93(B7)*, 7747–7766.

Serpelloni, E., M. Anzidei, P. Baldi, G. Casula, and A. Galvani (2005), Crustal velocity and strain-rate fields in Italy and surrounding regions: new results from the analysis of permanent and non-permanent GPS networks, *Geophysical Journal International, Vol. 161 (3)*, 861-880.

Serpelloni, E., G. Vannucci, S. Pondrelli, A. Argnani, G. Casula, M. Anzidei, P. Baldi, and P. Gasperini (2007), Kinematics of the Western Africa-Eurasia plate boundary from focal mechanisms and GPS data *Geophysical Journal International, 169 (3)*, 1180–1200.

Smith, A. D. and C. Lewis (1999), Differential rotation of lithosphere and mantle and the driving forces of plate tectonics, *Journal of Geodynamics*, *28*(2-3), 97-116.

Verdoya M., V. Pasquale, and P. Chiozzi (2005), Thermo-mechanical evolution and rheology of the northern sector of the Tyrrhenian–Apennines system, *Journal of Volcanology and Geothermal Research, 148 (1-2)*, 20-30.

1 Westaway, R. (1990), Present-day kinematics of the plate boundary zone between Africa and
2 Europe, from the Azores to the Aegean, *Earth and Planetary Science Letters, 96*, 393-406.

Figure Captions

Figure 1. Location map of the Central Mediterranean. Thick lines are the external thrusts and the thick arrow approximately represents the movement of Africa with respect to Europe. The codes at the edge indicate boundary conditions (see text for details).

Figure 2. Model grid (triangles), faults (thick lines), shear tractions locations (gray areas) and directions (arrows).

Figure 3. (A) Model misfit (I_s) for different sets of boundary conditions as a function of the shear tractions at the base of the model. (B) Average model misfit (histogram) and misfit RMS (error bars) of the best 50 models for different types of validation datasets in the "tractions" and "no tractions" scenarios.

Figure 4. Computed stress orientations (bars) and horizontal velocities (arrows) with (dark gray) and without (light gray) tractions, along with observed data (black) in the (A) Apennines and (B) Calabrian Arc. Data are from Montone et al. (2004), Serpelloni et al. (2007) and Caporali (2007).

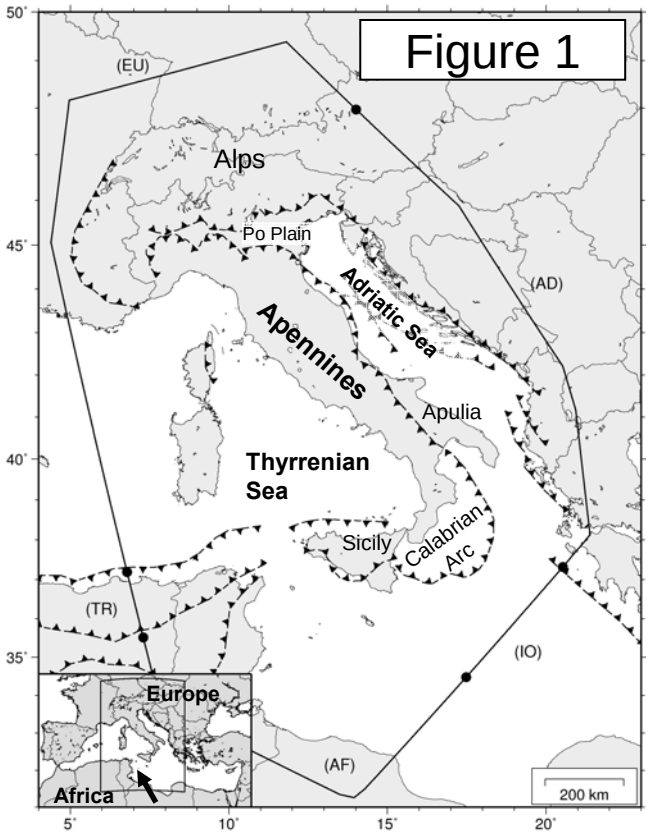
Figure 1
(EU)
Alps
Po Plain
Adriatic Sea
(AD)
Apennines
Apulia
Thyrrenian
Sea
Sicily
Calabrian
Arc
(TR)
(IO)
Europe
(AF)
Africa
200 km
50°
45°
40°
35°
5°
10°
15°
20°

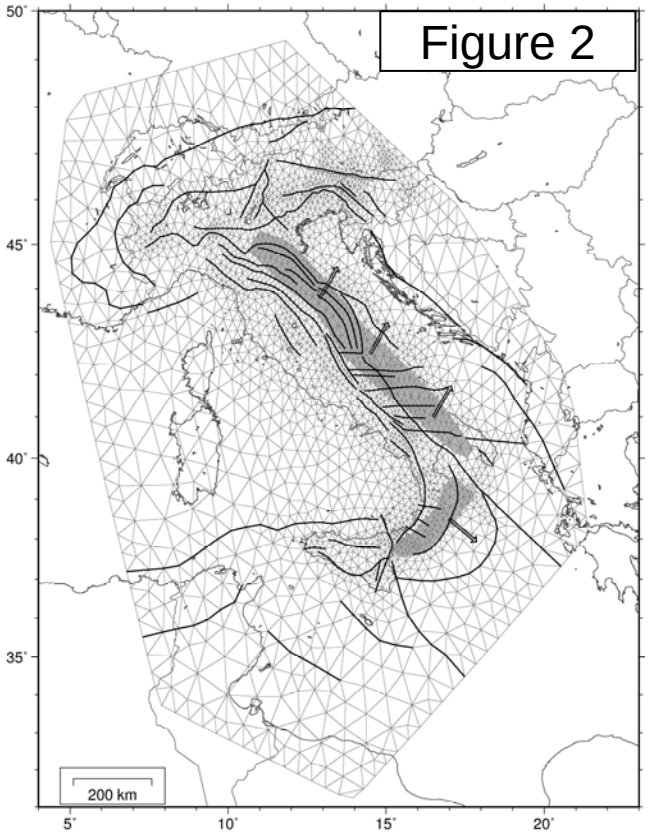
Figure 2
50°
45°
40°
35°
200 km
5°
10°
15°
20°

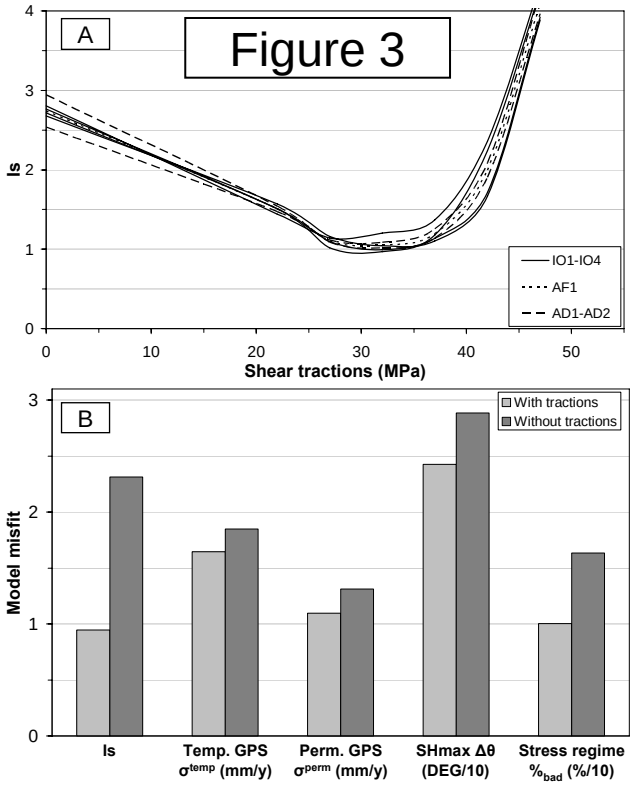
A
Figure 3
Is
Shear tractions (MPa)
IO1-IO4
AF1
AD1-AD2
B
Model misfit
With tractions
Without tractions
Is
Temp. GPS σ^temp (mm/y)
Perm. GPS σ^perm (mm/y)
SHmax Δθ (DEG/10)
Stress regime %bad (%/10)

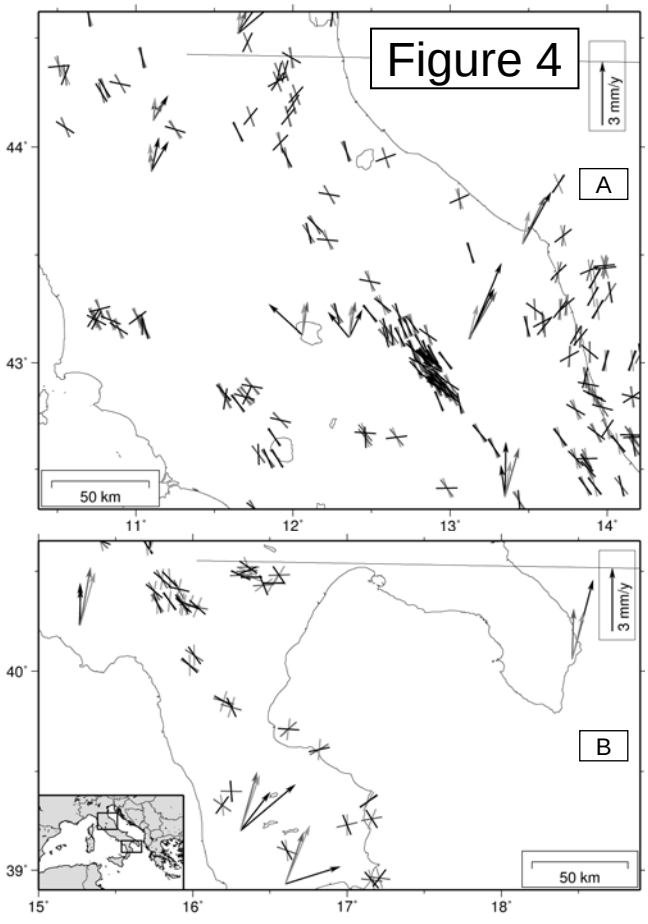
Figure 4
3 mm/y
A
50 km
44°
43°
11°
12°
13°
14°
3 mm/y
B
50 km
40°
39°
15°
16°
17°
18°

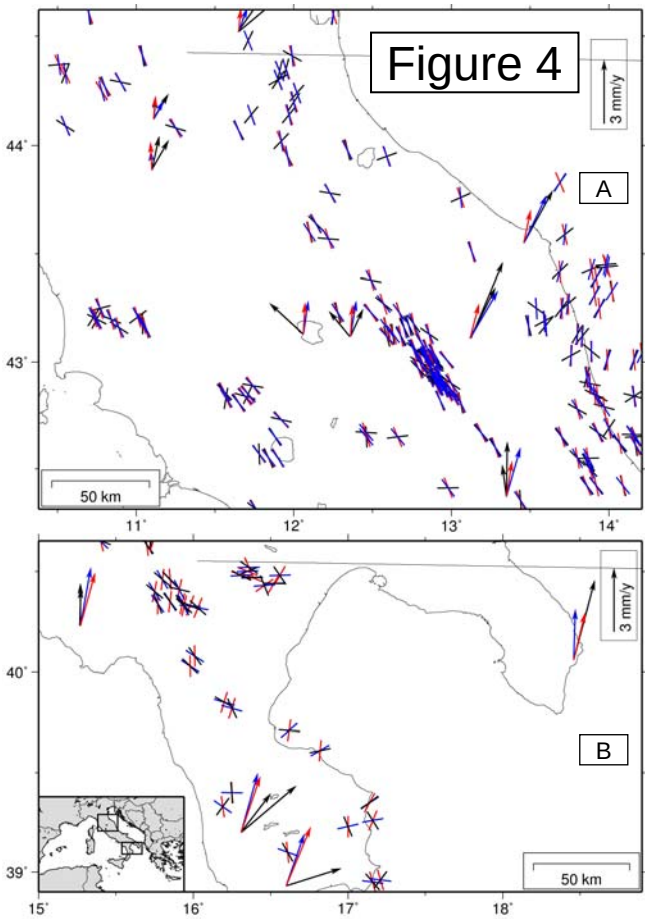
Figure 4
3 mm/y
A
44°
43°
50 km
11°
12°
13°
14°
3 mm/y
40°
B
39°
50 km
15°
16°
17°
18°